Superlight small bipolarons

2007 J. Phys.: Condens. Matter 19 255214

(http://iopscience.iop.org/0953-8984/19/25/255214)

IOP PUBLISHING JOURNAL OF PHYSICS: CONDENSED MATTER

J. Phys.: Condens. Matter **19** (2007) 255214 (26pp) doi:10.1088/0953-8984/19/25/255214

Superlight small bipolarons

J P Hague[1], P E Kornilovitch[2], J H Samson[1] and A S Alexandrov[1]

[1] Department of Physics, Loughborough University, Loughborough LE11 3TU, UK
[2] Hewlett-Packard Company, 1000 NE Circle Blvd, Corvallis, OR 97330, USA

Received 17 November 2006, in final form 19 February 2007
Published 30 May 2007
Online at stacks.iop.org/JPhysCM/19/255214

Abstract

Recent angle-resolved photoemission spectroscopy (ARPES) has identified that a finite-range Fröhlich electron–phonon interaction (EPI) with c-axis polarized optical phonons is important in cuprate superconductors, in agreement with an earlier proposal by Alexandrov and Kornilovitch. The estimated unscreened EPI is so strong that it could easily transform doped holes into mobile lattice bipolarons in narrow-band Mott insulators such as cuprates. Applying a continuous-time quantum Monte Carlo algorithm (CTQMC), we compute the total energy, effective mass, pair radius, number of phonons and isotope exponent of lattice bipolarons in the region of parameters where any approximation might fail, taking into account the Coulomb repulsion and the finite-range EPI. The effects of modifying the interaction range and different lattice geometries are discussed with regards to analytical strong-coupling/non-adiabatic results. We demonstrate that bipolarons can be simultaneously small and light, provided suitable conditions on the electron–phonon and electron–electron interactions are satisfied. Such light small bipolarons are a necessary precursor to high-temperature Bose–Einstein condensation in solids. The light bipolaron mass is shown to be universal in systems made of triangular plaquettes, due to a novel crab-like motion. Another surprising result is that the triplet–singlet exchange energy is of the first order in the hopping integral and that triplet bipolarons are much heavier than singlets in certain lattice structures. Finally, we identify a range of lattices where superlight small bipolarons may be formed, and give estimates for their masses in the anti-adiabatic approximation.

1. Introduction

A growing number of observations point to the possibility that high-T_c cuprate superconductors may not be conventional Bardeen–Cooper–Schrieffer (BCS) superconductors [1], but rather derive from the Bose–Einstein condensation (BEC) of real-space pairs, as proposed by Mott and others [2–5]. A possible fundamental origin of such strong departure of the cuprates from conventional BCS behaviour is the unscreened (Fröhlich) EPI with a polaron shift, E_p, of the order of 1 eV (La_2CuO_4, $E_p \approx 0.65$ eV) [6], routinely neglected in the Hubbard U and t–J models [7]. This interaction with c-axis polarized optical phonons is virtually unscreened

because the upper limit for the out-of-plane plasmon frequency ($\lesssim$200 cm^{-1} [8]) is well below the characteristic frequency of optical phonons, $\omega \approx$ 400–1000 cm^{-1}. Since screening is poor, the magnetic interaction remains small compared with the Fröhlich EPI at any doping of cuprates. In order to generate a convincing theory of high-temperature superconductivity, one must treat the Coulomb repulsion and *unscreened* EPI on an equal footing. When both interactions are strong compared with the kinetic energy of carriers, the so-called 'Coulomb–Fröhlich' model (CFM) predicts a ground state in the form of mobile, preformed, intersite pairs dressed by lattice deformations (i.e. intersite bipolarons) [6, 9, 4].

The most compelling evidence for (bi)polaronic carriers in novel superconductors is the discovery of a substantial isotope effect on the carrier mass [10] predicted by the bipolaron theory [11]. Recent high-resolution ARPES [12, 13] provides another piece of evidence for a strong EPI in cuprates between electrons and c-axis polarized optical phonons [13]. These, as well as recent tunnelling [14], earlier optical [15] and neutron scattering [16] experiments unambiguously show that lattice vibrations play a significant though unconventional role in high-temperature superconductors.

Remarkably, earlier path-integral studies of large bipolarons in the continuous limit [17] led to a double surprise:

(a) The large bipolaron is only stable in a very limited sector of the parameter space (Coulomb repulsion versus the Fröhlich coupling constant).
(b) Most traditional 'Fröhlich polaron' materials (alkali halides and the like) lie completely outside (and 'far' from) this bipolaron stability sector, but several high-T_c superconductors lie very close and even inside this rather restricted area of stability in the parameter space.

When the strong Fröhlich EPI operates together with a shorter-range deformation potential and molecular-type (e.g. Jahn–Teller) EPIs, it readily overcomes the Coulomb repulsion at short distances of about the lattice constant, so that large (continuous) bipolarons become local (lattice) bipolarons in narrow bands [4]. Even at significant doping local pairs are not overlapped, so a high critical temperature for Bose–Einstein condensation (BEC) could be achieved, if they are sufficiently mobile. Analysis of the site-local Holstein–Hubbard model has indicated that in order for the Coulomb repulsion (Hubbard U) to be overcome by the induced attractive force between electrons, the EPI must be so large that the polaron (and bipolaron) masses must be huge, rendering the transition temperature minuscule [18]. All is not lost, however, since the Holstein interaction is the extreme short-range limit of a finite-range EPI. Using the finite-range EPI, it is possible for electrons to pair between sites [6, 9] without requiring the electron–phonon-induced attraction to be larger than the Hubbard U. Moreover, the individual polarons are significantly lighter, so the mass of the pair has potential to be orders of magnitude smaller than in the Holstein case.

To put these arguments on a solid microscopic ground we simulate the CFM Hamiltonian on a lattice using an advanced QMC technique for bipolarons and compare with analytic results in the strong-coupling and anti-adiabatic limits. First, we introduce the model.

2. Coulomb–Fröhlich model

The Hamiltonian for the CFM is written as

$$H = -t \sum_{\langle \mathbf{n}\mathbf{n}'\rangle\sigma} c^{\dagger}_{\mathbf{n}'\sigma} c_{\mathbf{n}\sigma} + \tfrac{1}{2} \sum_{\mathbf{n}\mathbf{n}'\sigma\sigma'} V(\mathbf{n},\mathbf{n}') c^{\dagger}_{\mathbf{n}\sigma} c_{\mathbf{n}\sigma} c^{\dagger}_{\mathbf{n}'\sigma'} c_{\mathbf{n}'\sigma'} + \sum_{\mathbf{m}} \frac{\hat{P}^2_{\mathbf{m}}}{2M} + \sum_{\mathbf{m}} \frac{\xi^2_{\mathbf{m}} M\omega^2}{2} - \sum_{\mathbf{n}\mathbf{m}\sigma} f_{\mathbf{m}}(\mathbf{n}) c^{\dagger}_{\mathbf{n}\sigma} c_{\mathbf{n}\sigma} \xi_{\mathbf{m}}. \quad (1)$$

Each ion has a displacement $\xi_{\mathbf{m}}$. Site labels are $\mathbf{n}$ and $\mathbf{m}$ for electrons and ions respectively. The c annihilate electrons. The phonons are Einstein oscillators with frequency ω and mass M. The $\langle \mathbf{n}\mathbf{n}' \rangle$ denote pairs of nearest neighbours, and $\hat{P}_{\mathbf{m}} = -\mathrm{i}\hbar\partial/\partial\xi_{\mathbf{m}}$ ion momentum operators. The instantaneous interaction $V(\mathbf{n}, \mathbf{n}')$ has on-site repulsion U and nearest-neighbour interaction V (if the electron–phonon coupling term is set to zero, one obtains the simple UV model). The force function is of the screened Fröhlich type,

$$f_{\mathbf{m}}(\mathbf{n}) = \frac{\kappa}{[(\mathbf{m}-\mathbf{n})^2+1]^{3/2}} \exp\left(-\frac{|\mathbf{m}-\mathbf{n}|}{R_{\mathrm{sc}}}\right) \tag{2}$$

(κ is a constant) [20]. We will also use a slightly different notation for the electron–phonon interaction term here: $H_{\mathrm{el-ph}} = -\omega \sum_{ij\sigma} g_{ij} c^{\dagger}_{i\sigma} c_{i\sigma} (d^{\dagger}_j + d_j)$, where g_{ij} is a dimensionless interaction proportional to the force, and the $d^{\dagger}_j$ create phonons at site j. We set $\hbar = 1$.

Such a model has a remarkable property. Unlike the site-local Holstein model, there is attraction (and potentially pairing) even in the presence of very strong on-site Coulomb repulsion. The model is justified in the presence of alternating planes of itinerant electrons and ions, where there is strong screening along the c-axis.

There have been a number of studies discussing the masses of polarons and bipolarons with long-range interaction [19, 21, 22]. The polaron formed from the long-range Fröhlich interaction proposed in [6] has been simulated in [9], demonstrating that the polaron mass may be significantly lighter than its Holstein counterpart. This is due to the nature of polarons in the Holstein case, which may be demonstrated nicely by examining the Lang–Firsov transformation. In that transformation, the operators in the Hamiltonian are replaced in the following way:

$$d^{\dagger}_j \to \tilde{d}^{\dagger}_j = d^{\dagger}_j + \sum_i g_{ij} n_i \qquad c^{\dagger}_i \to \tilde{c}^{\dagger}_i = c^{\dagger}_i \exp\left[\sum_j g_{ij}(d^{\dagger}_j - d_j)\right] \tag{3}$$

$$d_j \to \tilde{d}_j = d_j + \sum_i g_{ij} n_i \qquad c_i \to \tilde{c}_i = c_i \exp\left[-\sum_j g_{ij}(d^{\dagger}_j - d_j)\right]; \tag{4}$$

thus hopping processes in the Holstein polaron (where $g_{ij} = g\delta_{ij}$) take place by a complete relaxation of the lattice on the initial site, a hop, and then a distortion on the target site. With a longer-range interaction, the lattice is pre-distorted before the particle moves, leading to a much smoother process with a lower intermediate energy state. We have recently determined that long-range interactions lead to a reduction of the importance of geometry on the properties of the polaron, especially the mass, leading to very similar results on triangular and square lattices [21]. We will discuss the crossover between Fröhlich and Holstein polarons later in this article.

The Lang–Firsov transformation is an exact canonical transformation, and leads to a transformed Hamiltonian with a new transformed wavefunction $|\Psi\rangle_{\mathrm{LF}} = \mathrm{e}^{-S}|\Psi\rangle$. It is most instructive to consider the transformation of the atomic Hamiltonian and the transformation of the hopping terms separately, since typically the Lang–Firsov transformation is the starting point for a series of perturbative analyses.

2.1. Transforming the atomic Hamiltonian

When the hopping term is set to zero, the phonon portion of the CFM is written as follows:

$$H_{\mathrm{at}} = -\omega \sum_{ij} g_{ij} n_i (d^{\dagger}_j + d_j) + \omega \sum_j \left(d^{\dagger}_j d_j + \tfrac{1}{2}\right). \tag{5}$$

(Note that the index i is now taken to contain a spin and a site index.) Applying the Lang–Firsov canonical transformation[3],

$$\tilde{H}_{\rm at} = -\omega \sum_{ij} g_{ij} n_i \left(d_j^\dagger + d_j + 2 \sum_{i'} g_{i'j} n_{i'} \right) + \omega \sum_j \left[\left(d_j^\dagger + \sum_i g_{ij} n_i \right) \left(d_j + \sum_{i'} g_{i'j} n_{i'} \right) + \tfrac{1}{2} \right] \tag{6}$$

$$= -\sum_{ii'} n_i n_{i'} \sum_j \frac{f_{ij} f_{i'j}}{2\omega^2 M} + \omega \sum_j \left(d_j^\dagger d_j + \frac{1}{2} \right), \tag{7}$$

where we reordered the summation, and noted that $g_{ij} = f_{ij}/\omega\sqrt{2M\omega}$. This shows the remarkable property of the Lang–Firsov transformation, since the electron and phonon subsystems in the atomic limit are now completely decoupled.

At this stage, it is convenient to introduce the following function,

$$\Phi_{\Delta \mathbf{r}}[\mathbf{r}(\tau), \mathbf{r}(\tau')] = \sum_{\mathbf{m}} f_{\mathbf{m}}[\mathbf{r}(\tau)] f_{\mathbf{m}+\Delta\mathbf{r}}[\mathbf{r}(\tau')], \tag{8}$$

where the reason for adding an additional translation, $\Delta\mathbf{r}$, to the phonon subsystem will become apparent when the action is introduced in the next section. For the following discussion, $\Delta\mathbf{r} = 0$. The Φ function for the ladder systems investigated in this paper is shown in figure 2, corresponding to a screened Fröhlich interaction with $R_{\rm sc} = 1$. We also define the dimensionless interaction parameter $\lambda = E_{\rm p}/W$, where W is the magnitude of the energy of the tight-binding electron (normally the half band width zt). As we can see from equation (7), the energy shift when there is only one particle (polaron shift for $i = i'$) is $E_{\rm p} = \frac{1}{2M\omega^2} \sum_j f_{0j}^2 = \frac{\Phi_0(0,0)}{2M\omega^2}$. Thus $\lambda = \frac{\Phi_0(0,0)}{2WM\omega^2}$. Substituting that definition into the atomic Hamiltonian, one obtains

$$\tilde{H}_{\rm at} = -\sum_{ii'} n_i n_{i'} \frac{W\lambda\Phi_0(i,i')}{\Phi_0(0,0)} + \omega \sum_j \left(d_j^\dagger d_j + \frac{1}{2} \right). \tag{9}$$

The reason for introducing the new functions Φ can immediately be seen, since they appear in the Hamiltonian as a ratio. Thus, in combination with λ they give a universal definition of coupling in models with long-range hopping.

2.2. *Transforming the electron hopping term*

Substitution of equations (3) and (4) transforms the tight-binding Hamiltonian in the following way:

$$H_{\rm tb} = \sum_{ii'} t_{ii'} c_i^\dagger c_{i'} \rightarrow \tilde{H}_{\rm tb} = \sum_{ii'} t_{ii'} \tilde{c}_i^\dagger \tilde{c}_{i'} = \sum_{ii'} \sigma_{ii'} c_i^\dagger c_{i'}, \tag{10}$$

where

$$\sigma_{ii'} = t_{ii'} \exp\left(\sum_j g_{ij} (d_j^\dagger - d_j) \right) \exp\left(-\sum_j g_{i'j} (d_j^\dagger - d_j) \right); \tag{11}$$

i.e. we can see that the electron–phonon interaction in the transformed Hamiltonian is part of the hopping process, and that, to some extent, one may regard the operators $\tilde{c}$ as creating polarons (i.e. electrons and a phonon cloud at the same time).

[3] Inspection of equations (3) and (4) shows that electron number operators are unchanged on transformation, so the Coulomb part of the Hamiltonian is also unchanged.

We now apply the following identity,

$$e^{A}e^{B}e^{-[A,B]/2} = e^{A+B} \tag{12}$$

(which is valid if $C = [A, B]$ commutes with both A and B) with $e^{-A}e^{A} = 1$, which is always valid. Therefore, $e^{A}e^{B} = e^{A+B}e^{[A,B]/2}$. In equation (11) we may choose $A = \sum_j g_{ij}(d_j^\dagger - d_j)$ and $B = -\sum_j g_{i'j}(d_j^\dagger - d_j)$. So, $A + B = \sum_j (g_{ij} - g_{i'j})(d_j^\dagger - d_j)$ and $[A, B] = 0$. Since the commutator is a number, equation (12) may be applied.

The hopping operator becomes

$$\sigma_{ii'} = t_{ii'} \exp\left(-\sum_j (g_{ij} - g_{i'j})d_j + \sum_j (g_{ij} - g_{i'j})d_j^\dagger\right). \tag{13}$$

Now, the identity may be used again, making the grouping $A = -\sum_j (g_{ij} - g_{i'j})d_j$ and $B = \sum_j (g_{ij} - g_{i'j})d_j^\dagger$. Thus $[A, B] = -\sum_j (g_{ij} - g_{i'j})(g_{ij} - g_{i'j})$, and

$$\sigma_{ii'} = t_{ii'} \exp\left[-\frac{W\lambda}{\omega}\left(1 - \frac{\Phi_0(i,i')}{\Phi_0(0,0)}\right)\right] \exp\left(\sum_j (g_{ij} - g_{i'j})d_j^\dagger\right) \exp\left(-\sum_j (g_{ij} - g_{i'j})d_j\right). \tag{14}$$

This form is particularly useful, due to the order of the creation and annihilation operators. Thus, when one carries out the perturbation theory, the calculation is reduced to computing matrix elements of the form $\langle l|(\sum_j (g_{ij} - g_{i'j})d_j^\dagger)^n (\sum_{j'} (g_{ij'} - g_{i'j'})d_{j'})^m |l'\rangle$. It is interesting to note that, when computed as an average over the atomic wavefunction, the hopping integral may be regarded as being modified by the EPI as $t_{ii'} \to t_{ii'} \exp(-W\lambda\gamma_{ii'}/\omega) = \tilde{t}_{ii'}$, where $\gamma_{ii'} = 1 - \Phi_0(i, i')/\Phi_0(0, 0)$. Such an approximation is valid in the anti-adiabatic limit, and will be revisited later in this paper. The band-narrowing factor was originally introduced by Tyablikov using an equations of motion scheme [24].

3. Quantum Monte Carlo simulation

The CTQMC algorithm presented here is an extension of a similar path-integral method for simulating the polaron problem [19]. An integration over phonon degrees of freedom following Feynman leads to an effective action, which is a functional of two polaron paths in imaginary time which form the bipolaron and is given by the following double integral when $\hbar\omega\beta \gg 1$ [22]:

$$\begin{aligned} A[\mathbf{r}(\tau)] = {} & \frac{z\lambda\bar{\omega}}{2\Phi_0(0,0)} \int_0^{\bar{\beta}} \int_0^{\bar{\beta}} d\tau\, d\tau' e^{-\bar{\omega}\bar{\beta}/2} \sum_{ij} \Phi_0[\mathbf{r}_i(\tau), \mathbf{r}_j(\tau')] \\ & \times \left(e^{\bar{\omega}(\bar{\beta}/2 - |\tau - \tau'|)} + e^{-\bar{\omega}(\bar{\beta}/2 - |\tau - \tau'|)}\right) \\ & + \frac{z\lambda\bar{\omega}}{\Phi_0(0,0)} \int_0^{\bar{\beta}} \int_0^{\bar{\beta}} d\tau\, d\tau' e^{-\bar{\omega}\tau} e^{-\bar{\omega}(\bar{\beta} - \tau')} \\ & \times \sum_{ij} \left(\Phi_{\Delta\mathbf{r}}[\mathbf{r}_i(\tau), \mathbf{r}_j(\tau')] - \Phi_0[\mathbf{r}_i(\tau), \mathbf{r}_j(\tau')]\right) \\ & - \tfrac{1}{2} \int_0^{\beta} V(\mathbf{r}_1(\tau), \mathbf{r}_2(\tau))\, d\tau, \end{aligned} \tag{15}$$

where the vector $\Delta\mathbf{r} = \mathbf{r}(\beta) - \mathbf{r}(0)$ is the difference between the end points of one of the paths in the non-exchanged configuration (here $\bar{\omega} = \hbar\omega/t$ and $\bar{\beta} = t/k_B T$). The indices $i = 1, 2$

and $j = 1, 2$ represent the fermion paths. $V(\mathbf{r}_1, \mathbf{r}_2)$ is an instantaneous Coulomb repulsion. The part of the action depending on $\Delta\mathbf{r}$ arises because the entire phonon subsystem at $\tau = \beta$ must also be shifted when there is a shift in the electron subsystem between the start and end configurations. The definition of $\Delta\mathbf{r}$ and other nomenclature for the CTQMC simulation of ladder systems are shown in figure 3.

From this starting point, the bipolaron is simulated using the Metropolis Monte Carlo (MC) method. The electron paths are continuous in time with hopping events (or kinks) introduced or removed from the path with each MC step. Analytic integration is performed over sections of parallel paths. The ends of the two paths at $\tau = 0$ and β are related by an arbitrary translation, $\Delta\mathbf{r}$. In contrast to the one-particle case, the fixing of the end configurations limits the update procedure to inserting and removing pairs of kinks and antikinks. We constrain particles to opposite legs of the ladder, which corresponds to two species of charged particles. In such a system, there is no exchange between particles. Exchange and singlet triplet splitting from quantum Monte Carlo simulations is briefly discussed in this section, with an analytical discussion in section 5. A full discussion of the QMC procedure for exchange is left to a future article.

3.1. Binary updates

In the path-integral QMC with two paths, it is necessary to make two kink operations simultaneously to ensure that the end configurations remain identical up to a translation. There exist two classes of update. First, kink/antikink pair addition/removal on a single path is useful, since it always maintains the same end configurations up to a change in the interpath displacement. Second, kink pair additions on different paths are needed in the analysis of the bipolaron mass, where the $\tau = \beta$ end configuration must be exactly equal to the $\tau = 0$ end configuration up to a parallel shift. Within both subclasses, there are two specific update types that satisfy the imaginary-time boundary conditions, as follows:

(I) Two kinks of the same type $\mathbf{l}$ are added to or removed from two different paths.
(II) A kink–antikink pair is added to or removed from one of the two paths. An antikink to kink $\mathbf{l}$ is a kink with the opposite direction $-\mathbf{l}$.
(III) A kink of type $\mathbf{l}$ is inserted into one path, and another kink of the same type $\mathbf{l}$ is removed from the same path (kink shift).
(IV) A kink of type $\mathbf{l}$ is added to one path, and an antikink $-\mathbf{l}$ is removed from the other path.

An important property of the bipolaron system is that the type and time of added or removed kinks still does not define the new path unambiguously. Indeed, imagine a kink of type $\mathbf{l}$ being inserted on a single path at time τ_{ins}. This could change the path in two different ways: either the path at times $\tau > \tau_{\text{ins}}$ is shifted in the direction $\mathbf{l}$, or the path at times $\tau < \tau_{\text{ins}}$ is shifted in the opposite direction. We refer to the former change as a top shift, and the latter as bottom shift. For the single-path (polaron) problem the distinction between the top and bottom shifts was not important because they are identical up to a translation of the entire path. This argument does not hold for two paths, since the resulting interpath distance in a binary update changes with shift type; thus a choice of shifts is an important part of the Monte Carlo update process. We proceed to derive the update probabilities for the Monte Carlo scheme set out above.

There is considerable flexibility in choosing the probabilities for adding and removing kinks. We choose an equal weighting scheme for choosing kinks, shifts and paths as follows:

(Ai) Choose a kink type $\mathbf{l}$ from the list of all possible kinks, with equal probability $P_{\mathbf{l}} = 1/N_k$, where N_k is the total number of kink types. $P_{\mathbf{l}}$ cancels on both sides of all balance equations considered below.

(Aii) Antikink types are always determined from the kink type.
(Aiii) Shift type (top or bottom) is chosen with equal probability $P_s = 1/2$ *independently* for the two kinks. P_s also cancels on both sides of the balance equation.
(Aiv) Assign path A with equal probability $1/2$ from the two available paths.
(Av) Assign path B as the other path.

We will also choose kinks to add and remove according to the following weightings, although there are some specific rules in the updates below to deal with cases where there are no kinks or antikinks of the chosen type on a path.

(Bi) The probability density for kink time selection when adding a kink is always $p(\tau) = 1/\beta$, $(0 < \tau < \beta)$.
(Bii) The probability for removing a kink of type $\mathbf{l}$ from path A in a configuration C is $1/N_{A\mathbf{l}}(C)$, where $N_{A\mathbf{l}}(C)$ is the number of kinks of type $\mathbf{l}$ on the path A.

We note that the following is not the only set of possible rules; however, we consider this to be the most transparent method of choosing kinks to insert and remove.

Update type (I): addition/removal of two kinks to or from different paths. Consider two configurations with two paths, C and D, where configuration D has two more $\mathbf{l}$ kinks than C, one on the first path at time τ_1, and one on the second path at time τ_2. The balance equation is

$$W(C)Q_A(C)P(C \to D) = W(D)Q_R(D)P(D \to C). \tag{16}$$

The relative weight of configurations C and D is $W(D)/W(C) = (t_\mathbf{l}\Delta\tau)^2 e^{A(D)-A(C)}$. In order to approach the limit of continuous time, we rewrite the probability Q_A of selecting two kinks at τ_1 and τ_2 to add to different paths given a configuration C as $Q_A(\mathbf{l}, \tau_1, A; \mathbf{l}, \tau_2, B|C) = q_A(\mathbf{l}, \tau_1, A; \mathbf{l}, \tau_2, B|C)(\Delta\tau)^2$, where q_A is the corresponding two-dimensional probability density. The probability of selecting the two specific kinks τ_1 and τ_2 to remove from the resultant configuration (D) to get back to C is a finite number $Q_R(\mathbf{l}, \tau_1, A; \mathbf{l}, \tau_2, B|D)$, which is the probability of removing those two kinks given configuration D. Substituting these results into the balance equation, one may cancel the $(\Delta\tau)^2$. Applying the Metropolis update scheme, probabilities are obtained as follows:

$$P(C \to D) = \min\left\{1; \frac{t_\mathbf{l}^2 Q_R(\mathbf{l}, \tau_1, A; \mathbf{l}, \tau_2, B|D)}{q_A(\mathbf{l}, \tau_1, A; \mathbf{l}, \tau_2, B|C)} e^{A(D)-A(C)}\right\}, \tag{17}$$

$$P(D \to C) = \min\left\{1; \frac{q_A(\mathbf{l}, \tau_1, A; \mathbf{l}, \tau_2, B|C)}{t_\mathbf{l}^2 Q_R(\mathbf{l}, \tau_1, A; \mathbf{l}, \tau_2, B|D)} e^{A(C)-A(D)}\right\}. \tag{18}$$

Thus we have obtained update probabilities that do not depend on the time discretization, and we can immediately take the limit of continuous time. A similar approach can be taken for any of the update types I–IV. We now demonstrate all steps in the derivation of the first update probability as an example.

The rules and resulting probabilities are as follows.

(i) Choose kink types, shifts and paths according to rules (Ai)–(Av).
(ii) If the initial configuration has *at least* one $\mathbf{l}$ kink on path A *and* on path B, then removal of a pair is proposed with probability $P_R = 1/2$, and addition of a pair is proposed with probability $P_A = 1/2$. Otherwise, only pair addition can be attempted and $P_A = 1$.
(iii) If pair addition is selected, times are selected to insert one kink on path A, and another on path B with independent equal probability density (rule (Bi)).

(iv) If pair removal is chosen, then one candidate kink is selected with independent equal probability from each of paths A and B in configuration D (rule (Bii)).

Implementing these choices, one obtains $q_{\mathrm{A}}(\mathbf{l}, \tau_1, A; \mathbf{l}, \tau_2, B|C) = P_{\mathbf{l}} P_{\mathrm{s}}^2 P_{\mathrm{A}}(C)/\beta^2$ from the combination of rules (i)–(iii). Likewise, the combination of rules (i), (ii) and (iv) specifies that $Q_{\mathrm{R}}(\mathbf{l}, \tau_1, A; \mathbf{l}, \tau_2, B|D) = P_{\mathbf{l}} P_{\mathrm{s}}^2 P_{\mathrm{R}}(D)/N_{\mathbf{l}A}(D) N_{\mathbf{l}B}(D)$. Rule (iii) leads to $P_{\mathrm{A}}(C) = 1/2$ if $N_{A\mathbf{l}}(C) \geqslant 1$ and $N_{B\mathbf{l}}(C) \geqslant 1$ and $P_{\mathrm{A}}(C) = 1$ otherwise. Since configuration D always has sufficient kinks to make a removal, we always have $P_{\mathrm{R}}(D) = 1/2$, leading to the following acceptance rules:

$$P(\text{addition}) = P(C \to D) = \min\left\{1; \frac{P_{\mathrm{R}}(D)(t_{\mathbf{l}}\beta)^2 \mathrm{e}^{A(D)-A(C)}}{P_{\mathrm{A}}(C) N_{A\mathbf{l}}(D) N_{B\mathbf{l}}(D)}\right\} \tag{19}$$

$$P(\text{removal}) = P(D \to C) = \min\left\{1; \frac{P_{\mathrm{A}}(C) N_{A\mathbf{l}}(D) N_{B\mathbf{l}}(D)}{P_{\mathrm{R}}(D)(t_{\mathbf{l}}\beta)^2 \mathrm{e}^{A(D)-A(C)}}\right\}. \tag{20}$$

Please note which configuration the kink numbers apply to. In the case of kink addition, the initial configuration is C and final configuration is D. In the case of kink removal, the initial configuration is D and the final configuration is C.

Update type (II): addition/removal of a kink–antikink pair to one path. The general properties of this update type are similar to update type (I): the addition of a pair at times τ_1 and τ_2 is characterized by a two-dimensional probability density $q_{\mathrm{A}}(\mathbf{l}, \tau_1, A; -\mathbf{l}, \tau_2, A|C)$, while removal of a pair is characterized by a finite number $Q_{\mathrm{R}}(\mathbf{l}, \tau_1, A; \mathbf{l}, \tau_2, A|D)$. Equations (17) and (18) still apply with $t_{\mathbf{l}} t_{-\mathbf{l}}$ in place of $t_{\mathbf{l}}^2$. Since $t_{\mathbf{l}} = t_{-\mathbf{l}}$, the acceptance rules are identical, and only Q and q differ.

We use the following rules.

(i) Choose kink types, shifts and paths according to rules (Ai)–(Av).
(ii) If the initial configuration has *at least* one $\mathbf{l}$ kink and one antikink ($N_{A\mathbf{l}} \geqslant 1$, $N_{A-\mathbf{l}} \geqslant 1$), then removal of a pair is proposed with probability $P_{\mathrm{R}} = 1/2$, and addition of a pair is proposed with probability $P_{\mathrm{A}} = 1/2$. Otherwise, addition of a pair is proposed with probability $P_{\mathrm{A}} = 1$.
(iii) If pair addition is selected, kink and antikink insertion times are selected with independent equal probability density for insertion on path A (rule (Bi)).
(iv) If pair removal is chosen, then one candidate kink and one candidate antikink are selected with independent equal probability from path A in configuration D (rule (Bii)).

One computes the update probabilities as before:

$$P(\text{addition}) = P(C \to D) = \min\left\{1; \frac{P_{\mathrm{R}}(D)(t_{\mathbf{l}}\beta)^2 \mathrm{e}^{A(D)-A(C)}}{P_{\mathrm{A}}(C) N_{A\mathbf{l}}(D) N_{A-\mathbf{l}}(D)}\right\} \tag{21}$$

$$P(\text{removal}) = P(D \to C) = \min\left\{1; \frac{P_{\mathrm{A}}(C) N_{A\mathbf{l}}(D) N_{A-\mathbf{l}}(D)}{P_{\mathrm{R}}(D)(t_{\mathbf{l}}\beta)^2 \mathrm{e}^{A(D)-A(C)}}\right\}. \tag{22}$$

Update type (III): addition and removal of a kink to one path (kink shift). This update type does not change the number of kinks, and hence does not change the kinetic energy of the system. We define a configuration C, and a configuration D which is identical to C except that one kink has been shifted. To get from configuration C to D, a kink is removed from path A at time τ_1 and is reinserted in the path at time τ_2. Since C and D have equal total kink number, the ratio of statistical weights is $W(D)/W(C) = \mathrm{e}^{A(D)-A(C)}$. From detailed balance and the Metropolis update scheme,

$$P(C \to D) = \min\left\{1;\ \frac{Q_{\mathrm{R}}(\mathbf{l}, \tau_2, A|D) q_{\mathrm{A}}(\mathbf{l}, \tau_1, A|D)}{Q_{\mathrm{R}}(\mathbf{l}, \tau_1, A|C) q_{\mathrm{A}}(\mathbf{l}, \tau_2, A|C)} \mathrm{e}^{A(D)-A(C)}\right\}. \tag{23}$$

There is only one update rule, since we can get from D and C using exactly the same process as going from C to D. All attributes of the kinetic energy have dropped out from the equations. The acceptance rules are determined solely by the electron–phonon interaction, as expected for this update type.

In many practical situations it is reasonable to choose the functions q and Q independent of time τ. In this case the above expressions simplify significantly. In particular, consider the following set of update rules.

(i) Choose kink types, shifts and paths according to the general rules (Ai)–(Av).
(ii) If the path has no $\mathbf{l}$ kinks, $N_{\mathbf{l}} = 0$, the update attempt is aborted. Otherwise, $N_{\mathbf{l}} \geqslant 1$, so propose an $\mathbf{l}$ kink for removal with equal probability $1/N_{\mathbf{l}}(C)$ (rule (Bii)).
(iii) Propose a time for a new $\mathbf{l}$ kink with constant probability density $p(\tau) = 1/\beta$ (rule (Bi)).

These rules result in cancellation of Q_{remove} and q_{add} from the above equations, which reduce to

$$P(C \to D) = \min\left\{1; \mathrm{e}^{A(D)-A(C)}\right\}. \tag{24}$$

Update type (IV): kink addition to one path and antikink removal from the other path. In this update, a kink $\mathbf{l}$ is added to one path and an antikink $-\mathbf{l}$ is removed from the other path. As a result, the β end configuration shifts as a whole by $\mathbf{l}$. In a reciprocal process, a kink $\mathbf{l}$ is removed from one path, an antikink $-\mathbf{l}$ is inserted in the other path, and the β configuration shifts by $-\mathbf{l}$.

The ratio of weights is $W(D)/W(C) = (t_{-\mathbf{l}}/t_{\mathbf{l}})\mathrm{e}^{A(D)-A(C)}$. The balance equation is satisfied by the following solution:

$$P(C \to D) = \min\left\{1;\ \frac{Q_{\mathrm{R}}(\mathbf{l}; \tau_1; A|D) q_{\mathrm{A}}(-\mathbf{l}; \tau_2; B|D)}{Q_{\mathrm{R}}(-\mathbf{l}; \tau_2; B|C) q_{\mathrm{A}}(\mathbf{l}; \tau_1, A|C)} \mathrm{e}^{A(D)-A(C)}\right\}. \tag{25}$$

Since we can obtain the inverse process by changing kink $\mathbf{l}$ for its antikink, the update probability $P(D \to C)$ is not necessary since we always choose $\mathbf{l}$ from all kink types.

As the simplest implementation, the following rules are used.

(i) Choose kink types, shifts and paths according to rules (Ai)–(Av).
(ii) If path B has no antikinks $-\mathbf{l}$, $N_{B-\mathbf{l}} = 0$, then the update attempt is aborted. Otherwise, $N_{B-\mathbf{l}} \geqslant 1$, so an antikink is proposed for removal from path B with equal probability (rule (Bii)).
(iii) The time location for kink insertion on path A is proposed with equal probability density (rule (Bi)).

With these choices, the acceptance probability takes the form

$$P(C \to D) = \min\left\{1;\ \frac{N_{B-\mathbf{l}}(C)}{N_{A\mathbf{l}}(D)} \mathrm{e}^{A(D)-A(C)}\right\}. \tag{26}$$

3.2. Estimators

When our Monte Carlo scheme has reached equilibrium, we make a series of measurements of physical properties. The ground state energy is

$$\epsilon_0 = -\lim_{\beta\to\infty}\left[\left\langle\frac{\partial A}{\partial\beta}\right\rangle - \frac{1}{\beta}\left\langle\sum_{\mathrm{s}} N_{\mathrm{s}}\right\rangle\right], \tag{27}$$

where N_s is the number of kinks of type s, and angular brackets denote ensemble averaging. The number of phonons is given by

$$N_{\rm ph} = -\lim_{\beta\to\infty} \frac{1}{\bar{\beta}} \left\langle \left. \frac{\partial A}{\partial \bar{\omega}} \right|_{\lambda\bar{\omega}} \right\rangle, \tag{28}$$

where the derivative is taken keeping $\lambda\bar{\omega}$ constant. The polaron band energy spectrum can be computed from

$$\epsilon_{\mathbf{k}} - \epsilon_0 = -\lim_{\beta\to\infty} \frac{1}{\beta} \ln\langle\cos(\mathbf{k}\cdot\Delta\mathbf{r})\rangle, \tag{29}$$

where $\mathbf{k}$ is the quasi-momentum. By expanding this expression in small $\mathbf{k}$, the ith component of the inverse effective mass is obtained as

$$\frac{1}{m_i^*} = \lim_{\beta\to\infty} \frac{1}{\beta\hbar^2} \langle(\Delta\mathbf{r}_i)^2\rangle. \tag{30}$$

Thus the inverse effective mass is the diffusion coefficient of the polaron path in the limit of the infinitely long 'diffusion time', β. The bipolaron radius is the average distance between paths,

$$R_{\rm bp} = \left\langle \sqrt{\frac{1}{\beta}\int_0^\beta \Delta\mathbf{r}_{12}(\tau)^2\,{\rm d}\tau} \right\rangle. \tag{31}$$

Finally, the mass isotope coefficient, $\alpha_{m_i^*} = {\rm d}\ln m_i^*/{\rm d}\ln M$, is calculated as follows:

$$\alpha_{m_i^*} = \lim_{\beta\to\infty} \frac{\bar{\omega}}{2} \frac{1}{\langle(\Delta\mathbf{r}_i)^2\rangle} \left[\left\langle (\Delta\mathbf{r}_i)^2 \left. \frac{\partial A}{\partial\bar{\omega}} \right|_\lambda \right\rangle - \langle(\Delta\mathbf{r}_i)^2\rangle \left\langle \left. \frac{\partial A}{\partial\bar{\omega}} \right|_\lambda \right\rangle \right]. \tag{32}$$

3.3. General Monte Carlo considerations

There are certain aspects of good practice for quantum Monte Carlo simulations that we adhere to here. As always for Monte Carlo simulations, a random number generator with sufficient period is used. Measurements are performed every few steps to avoid unnecessary correlations in results (the aim here is to spend no longer measuring than simulating, since time-correlated results do not make a large contribution to more accurate measurement). Careful blocking analysis with large blocking sizes $N_{\rm B}$ is performed to determine accurate error bars. To avoid anomalous error bars caused by long time correlations, we compare error bars computed with two block sizes, $N_{\rm B}$ and $2N_{\rm B}$.

3.4. Exchanges

Exchanges are significantly more complicated, with several possibilities for the exchange update involving inserting and removing kinks. In the exchanged configuration, there are an additional four update rules, and there is also an ambiguous configuration where both paths have the same start and end points, which leads to some small additional modifications. We defer a full discussion of exchange update rules to a later paper. On our ladder models, exchanges are not required, since electrons sit on opposite legs.

3.5. Singlet–triplet splitting in the Monte Carlo method

A consequence of exchange is that singlet and triplet states are not degenerate. We can see the singlet–triplet mass difference as a consequence of interference between paths in the Monte Carlo simulation. We take a simplified one-dimensional example to illustrate the mechanism. Consider a bipolaron of separation R propagating from the sites $\{0, R\}$ at $\tau = 0$ to $\{\Delta r, R+\Delta r\}$

at $\tau = \beta$. We assume that the weight w of a single-electron path is a monotonically decreasing function of the number n of kinks in the path, and the paths with the smallest number of kinks dominate. This is likely to be valid in the strong-coupling limit. We can therefore write the weight of a path as a monotonically rapidly decreasing function $w(d)$, where d is the distance between endpoints. We also neglect the interaction between paths.

Consider first the case of periodic boundary conditions $\Delta r = 0$. The weights of the singlet and triplet bipolaron paths are respectively the sum and the difference of the direct and exchange paths.

$$w_{\mathrm{s}}(0) \approx w(0)w(0) + w(R)w(R), \tag{33}$$

$$w_{\mathrm{t}}(0) \approx w(0)w(0) - w(R)w(R). \tag{34}$$

Here, if $w(R) \ll w(0)$, the singlet and triplet weights are dominated by the direct path and are nearly equal.

Now consider a twist larger than the bipolaron radius, $\Delta r > R > 0$. The singlet and triplet weights are dominated by the shortest paths:

$$w_{\mathrm{s}}(0) = w(\Delta r)w(\Delta r) + w(\Delta r + R)w(\Delta r - R), \tag{35}$$

$$w_{\mathrm{t}}(0) = w(\Delta r)w(\Delta r) - w(\Delta r + R)w(\Delta r - R). \tag{36}$$

In this case the total number of kinks in either the direct or the exchange path is the same ($2\Delta r$), so there will be substantial cancellation in the triplet case. Thus the diffusion coefficient of the triplet bipolaron will be smaller, and the effective mass larger, than that of the singlet.

4. Polarons on triangular and rectangular systems

We briefly discuss the lattice-dependent features of the polaron problem here. For more detailed discussion of the polaron problem, the reader is directed towards our papers on this subject [21, 20, 19], and to the paper by Kornilovitch in this issue [26]. In this section, we specifically discuss the changes to the masses of polaron moving on triangular and square lattices as the screening length R_{sc} is varied. The polaron mass forms part of the argument later in this article.

Screened Fröhlich electron–phonon interactions were simulated by Spencer *et al* [20], who demonstrated a continuous crossover between the Fröhlich and Holstein limits on the chain. In particular, the mass of the particle is found to be light down to quite small screening radii, consistent with results by Bonča and Trugman [18] for nearest-neighbour electron–phonon interactions.

We have previously computed the properties of polarons on several Bravais lattices, showing that the effects of the lattice type on the properties of the polaron are 'washed out' by long-range interactions [21]. Figure 4 shows the effective mass of the discrete Fröhlich polaron on square and triangular lattices. Fröhlich polarons are significantly lighter than their Holstein counterparts, due to the long-range interaction. We have also shown that the overriding factor for the properties of Holstein polarons is the number of nearest neighbours in the lattice, and not the dimensionality [21]. Since we are interested in long-range interactions in this paper, then it suffices to note that the masses of Fröhlich polarons are of the same order of magnitude on all lattice types, and that they are extremely light [21]. The properties of realistic screened interactions lie somewhere in between, but such polarons remain light down to quite small interaction ranges of the order of a lattice spacing [20].

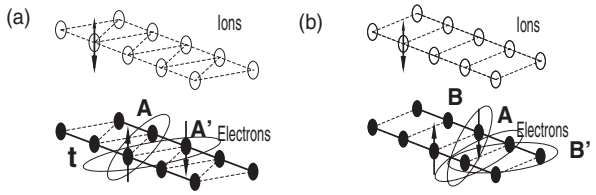

Figure 1. (a) Staggered versus (b) rectangular ladders. Ions are placed one lattice spacing above a ladder of electrons, with one ion per site. The ions are permitted to vibrate in the z-direction only. Electrons inhabit one leg each, with no hopping between the legs. In the strong-coupling limit, there are significant geometrical differences. On the staggered ladder, two degenerate near-neighbour pairs (A and A′) can form, which allows the polaron to scuttle in a crab-like manner with mass proportional to the polaron hopping. Alternatively, on the rectangular ladder there is one near-neighbour state, and in order to move, the pair must break to state A in order to change configuration from state B to B′. Such a state propagates by waddling awkwardly, and has mass proportional to polaron hopping squared.

5. Bipolarons on ladder systems

The properties of bipolarons are significantly more complicated than those of polarons. One expects bound Holstein bipolarons in strongly correlated materials to be extremely heavy, since a very large attractive potential is needed to overcome the repulsion. This is not true for longer-range interactions. According to work by Bonča and Trugman [18], even bipolarons with nearest-neighbour interactions are significantly more mobile than their Holstein counterparts (indeed, one normally expects the mass of a bipolaron to scale like the squared mass of the polaron, so polarons which are an order of magnitude lighter than Holstein ones may become bipolarons which are two orders of magnitude lighter). Another extremely interesting proposition is the role of geometry on the bipolaron mass. When bipolarons are bound on nearest-neighbour sites, and another degenerate state may be reached in a single hopping event, the leading correction to the atomic Hamiltonian is first order in the hopping term, and not second order as one might expect for the Holstein model, which leads to a bipolaron with a mass that is of similar order of magnitude to the polaron mass (i.e. a superlight bipolaron) [9]. Such systems may be realized on triangular lattices, or on lattices with large next-nearest neighbour hopping. We have recently extended our quantum Monte Carlo algorithm to explore this type of bipolaron, leading to similar conclusions [22]. In this paper, we discuss some of these extensions to the algorithm to look at two types of ladder system shown in figure 1.

5.1. Weak and strong coupling

Since the particles on the different legs of the ladder cannot exchange, the very weak-couping limit is not well bound, consisting of two large polarons. As such a weak coupling perturbation expansion can be constructed around the unbound state. As will become apparent when we show the quantum Monte Carlo results, the number of phonons is small for the weakly bound states, especially in the anti-adiabatic limit. The perturbation theory in the electron–phonon coupling term only excites single phonons, so if the number of phonons becomes too large, the theory fails. In the presence of strong on-site repulsion, the bipolaron is not bound at zero coupling. In general, if there is a bound state for $\lambda \to 0^+$, then this perturbation expansion fails. The expansion is written as follows:

$$E_{\mathbf{k}} = 2\epsilon_{\mathbf{k}}^{(0)} - 2\frac{\lambda\omega W}{\Phi_0(0,0)}\frac{1}{N}\sum_{\mathbf{q}}\frac{|f_{\mathbf{q}}|^2}{W(\mathbf{k},\mathbf{q})}, \tag{37}$$

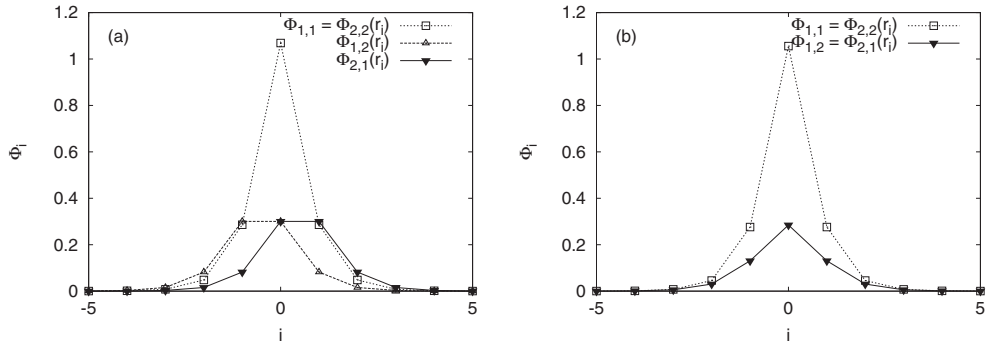

Figure 2. Φ functions for (a) the staggered ladder and (b) the rectangular ladder (subscripts 1 and 2 correspond to the leg of the chain). Note that since an index is assigned to each unit cell, there is an offset of one lattice index, i, in the interaction function between paths on legs 1 and 2, relative to the interaction function between legs 2 and 1 when the staggered ladder is simulated. Here $R_{sc} = 1$.

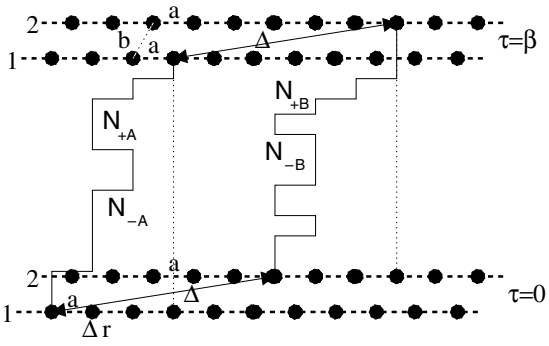

Figure 3. Example path configuration on the ladder system, showing the notation used. Paths are separated by a vector **b**, and sites in the chain by **a**. The path configuration at $\tau = 0$ is identical to that at $\tau = \beta$ up to a shift Δr (i.e. the ends of the beginning and end of the paths are separated by Δ). Each path has a number of kinks $N_{A/B+}$ and antikinks $N_{A/B-}$.

$$W(\mathbf{k}, \mathbf{q}) = \epsilon^{(0)}_{\mathbf{k}-\mathbf{q}} + \omega - \epsilon^{(0)}_{\mathbf{k}}, \tag{38}$$

$$f_{\mathbf{q}} = \sum_{\mathbf{m}} f_{\mathbf{m}}(0) \mathrm{e}^{-\mathrm{i}\mathbf{q}\cdot\mathbf{m}}, \tag{39}$$

where N is the number of momentum states. Thus the ground-state polaron energy (at $\mathbf{k} = 0$) is $\epsilon^{(2)}_0 = -W + \lambda W \Gamma_{\epsilon_0}(\bar{\omega})$, which defines a dimensionless coefficient Γ_{E_0}.

There is no general analytic solution for the second-order perturbation theory, but values may be computed using numerical integration. The number of phonons, isotope exponent and inverse mass may also be written as $N_{\mathrm{ph}} = 2\lambda\Gamma_N(\hbar\omega)$, $\alpha = 2\lambda\Gamma_\alpha(\hbar\omega)$ and $2m_0/m^{**} = 1 - \Gamma_m(\hbar\omega)\lambda$. The weak-coupling limits for the polaron are discussed in [20, 21] among others. λ is defined as before.

Aspects of the strong-coupling limit are easy to compute from the path-integral formalism. In the very-strong-coupling limit, the most common configurations are straight paths, since the action is proportional to λ and that configuration gives the smallest possible action. Thus the

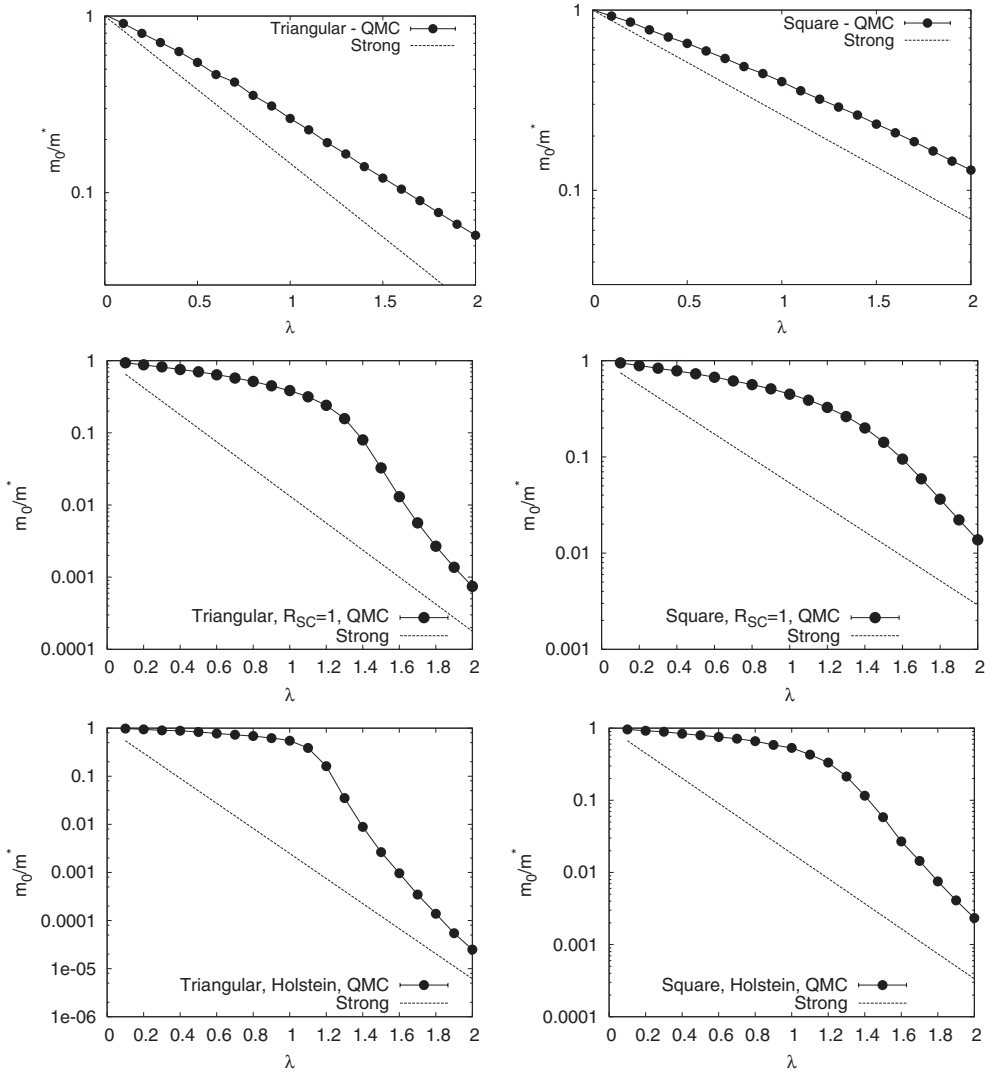

Figure 4. Inverse effective mass of the discrete Fröhlich polaron on square and triangular lattices. $\omega/t = 1$, and λ is varied. Triangular lattices are shown on the left, and square lattices are shown on the right. From top to bottom, the screening radius of the interaction is decreased, with the top graphs showing Fröhlich interaction $R_{sc} \to \infty$, the middle graphs screened interaction $R_{sc} = 1$ and the bottom graphs the Holstein interaction $R_{sc} = 0$. Fröhlich polarons are significantly lighter than their Holstein counterparts because the long-range interaction leads to pre-distortions of the lattice before a hopping.

strong-coupling action reads

$$A_{\text{strong}} = \frac{\lambda W(\hbar\omega\beta - 1 + \mathrm{e}^{-\hbar\omega\beta})}{\Phi_0(0,0)\hbar\omega} \sum_{ij} \Phi_0(i,j). \tag{40}$$

For a polaron, the total energy for a self-interacting strong-coupling system (i.e. a straight path) is $E = -W\lambda$, where W is the half band width, $-\epsilon_{\mathbf{k}=0}$. Computing the action for the straight

Table 1. Strong-coupling behaviour of the staggered and rectangular lattices. Here, $R_{sc} = 1$.

Lattice	$\Phi(0,0)$	$\Phi(0,\mathbf{b})$	$1+\frac{\Phi(0,\mathbf{b})}{\Phi(0,0)}$	$E/W\lambda$	$\bar{\omega}N_{ph}/\lambda$
Staggered	1.068 96	0.300 34	1.280 96	−5.123 84	5.123 84
Rectangular	1.055 54	0.284 832	1.269 84	−5.079 36	5.079 36

path configuration, one obtains the energy as $E_{strong} = -\partial A_{strong}/\partial\beta|_{\beta\to\infty}$. This leads to

$$E^{bp}_{strong} = -2W\lambda[1 + \Phi_0(0,\mathbf{b})/\Phi_0(0,0)], \tag{41}$$

where $\mathbf{b}$ is a nearest-neighbour vector between chains indicating the point of closest approach. This result is of little surprise, since there are two polarons in a bipolaron, with $E = -W\lambda$ each, and two inter-polaron binding terms with $E = -W\lambda\Phi(0,\mathbf{b})/\Phi(0,0)$. We may also compute the number of phonons associated with the bipolaron in a similar manner, using equation (28) with A_{strong}, which we obtain as

$$N^{ph}_{strong} = 2W\lambda[1 + \Phi(0,\mathbf{b})/\Phi(0,0)]/\hbar\omega. \tag{42}$$

As we have discussed, the Φ functions for the ladder systems with $R_{sc} = 1$ are plotted in figure 2. Numerical values for $\Phi(0,\mathbf{b})$, $\Phi(0,0)$ and $1+\Phi(0,\mathbf{b})/\Phi(0,0)$ are shown in table 1, from which numerical values for the strong-coupling behaviour are computed. We discuss the region of validity of these results when we compute the exact QMC results. In particular, if we plot appropriate ratios, such as the ratio $N_{ph}\bar{\omega}/\lambda$, we expect saturation at strong coupling, consistent with table 1.

Typically, it has been discussed that an expansion of the Lang–Firsov transformed Hamiltonian in the polaron hopping can be used at strong coupling. The perturbation expansion to second order may be written as

$$E_{tot} = E_{at} + \langle\Psi|\tilde{H}_{tb}|\Psi\rangle_{at} + \sum_j \frac{|\langle\Phi_j|\tilde{H}_{tb}|\Psi_{at}\rangle|^2}{E_j - E_{at}}. \tag{43}$$

The values for the strong-coupling energy may be computed from the leading term of this expansion, and they have the same form as the energy computed from the straight paths. This is not surprising, since the corrections to the energy are at least as small as $\tilde{t}$.

There is a subtle point associated with phonon numbers. By examination, the ground state of the phonon subsystem in the *transformed* Hamiltonian is $\sum_j d^\dagger_j d_j = \sum_j n_j = 0$. In order to determine the total number of phonons in the true ground state of the atomic Hamiltonian, one must transform back to the regular wavefunction. One may either transform the wavefunction, or the phonon part of the Hamiltonian. Transforming the phonon part of the Hamiltonian is easy, and one obtains

$$\langle\phi_{LF}|\tilde{H}_{ph}|\phi_{LF}\rangle = \langle\phi|H_{ph}|\phi\rangle = \omega N_{ph}; \tag{44}$$

thus

$$N_{ph} = \langle\phi_{LF}|\sum_j \left(d^\dagger_j + \sum_i g_{ij}n_i\right)\left(d_j + \sum_{i'} g_{i'j}n_{i'}\right)|\phi_{LF}\rangle/\omega \tag{45}$$

$$= \langle\phi_{LF}|\sum_{ii'j} g_{ij}g_{i'j}n_i n_{i'}|\phi_{LF}\rangle/\omega. \tag{46}$$

The expectation value of the phonon's occupation may be rewritten in terms of λ and Φ; thus

$$N_{ph} = -\frac{E_{at}}{\omega}. \tag{47}$$

(Note the minus sign in front of the equation: the phonon number is positive.)

Thus one determines that the total number of phonons in the bipolaron case is

$$N_{\mathrm{ph,at}} = \frac{2W\lambda}{\omega}\left(1 + \frac{\Phi_0(0,\mathbf{b})}{\Phi_0(0,0)}\right). \tag{48}$$

(Note that a similar argument can be used for polarons.)

Unfortunately, the computation of the mass is not so simple. The mass is very sensitive to the exact form of the renormalized hopping, and the leading order of the perturbation expansion varies with lattice type. For the superlight small bipolarons on triangular plaquettes discussed here, there is a leading term with order $\tilde{t}$, and for rectangular systems, the leading order is $\tilde{t}^2$. Examination of the path integrals demonstrates that the mass is computed from a parallel shift. The first perturbation of the paths from the straight line in the atomic limit is the insertion of two parallel kinks (one on each path). In order for the mass to be genuinely first order in the polaron hopping, we would require updates with only one kink. Thus, there are significant contributions from the second-order term, including a cancellation between the orders as $\lambda \to \infty$. In fact, the expansion of the Lang–Firsov transformed Hamiltonian to first order in the hopping turns out to correspond to the extreme anti-adiabatic limit, which we now discuss.

5.2. Anti-adiabatic approximation

The bipolaron dispersion can be evaluated analytically in the anti-adiabatic strong-coupling limit ($\hbar\omega \gg t, \lambda \gg 1$), in which case the problem can be reduced to that of a rigid dimer. In this limit the Lang–Firsov transformation [23] eliminates the phonons from the Coulomb–Fröhlich Hamiltonian (1). In combination with an averaging over phonons consistent with the anti-adiabatic approximation (if the phonon frequency is very large, there are no real phonons) one obtains the following effective UV Hamiltonian:

$$\begin{aligned}\tilde{H} = &-\sum_{\mathbf{n}\mathbf{n}'\sigma} \tilde{t}_{\mathbf{n}\mathbf{n}'} c^{\dagger}_{\mathbf{n}\sigma} c_{\mathbf{n}'\sigma} - E_{\mathrm{p}} \sum_{\mathbf{n}\sigma} c^{\dagger}_{\mathbf{n}\sigma} c_{\mathbf{n}\sigma} \\ &+ \tilde{U} \sum_{\mathbf{n}} c^{\dagger}_{\mathbf{n}\uparrow} c_{\mathbf{n}\uparrow} c^{\dagger}_{\mathbf{n}\downarrow} c_{\mathbf{n}\downarrow} + {\sum_{\mathbf{n}\mathbf{n}'}}' \sum_{\sigma\sigma'} \tilde{V}_{\mathbf{n}\mathbf{n}'} c^{\dagger}_{\mathbf{n}\sigma} c_{\mathbf{n}\sigma} c^{\dagger}_{\mathbf{n}'\sigma'} c_{\mathbf{n}'\sigma'},\end{aligned} \tag{49}$$

where the primed sum excludes self-interaction, and the renormalized on-site and intersite interactions are

$$\tilde{U} = \frac{V(\mathbf{0},\mathbf{0})}{2} - W\lambda \tag{50}$$

and

$$\tilde{V}_{\mathbf{n}\mathbf{n}'} = \frac{V(\mathbf{n},\mathbf{n}')}{2} - \frac{W\lambda\Phi_{\mathbf{0}}(\mathbf{n},\mathbf{n}')}{\Phi_{\mathbf{0}}(\mathbf{0},\mathbf{0})} \tag{51}$$

respectively. (There is no retardation in the anti-adiabatic limit.) Now suppose the on-site repulsion $\tilde{U} \gg \tilde{t}$ is large and repulsive and the intersite interaction has a well-defined minimum $V_{\min} < 0$ at some separation. Let $N_{\mathbf{n}}$ be the set of sites of $\mathbf{n}'$ at that separation from $\mathbf{n}$:

$$N_{\mathbf{n}} = \{\mathbf{n}' : \tilde{V}_{\mathbf{n}\mathbf{n}'} = V_{\min}\} \tag{52}$$

and

$$\tilde{V}_{\mathbf{n}\mathbf{n}'} - V_{\min} \gg \tilde{t} \qquad \text{for } \mathbf{n}' \notin N_{\mathbf{n}}. \tag{53}$$

We shall call $N_{\mathbf{n}}$ the 'neighbours' of $\mathbf{n}$. In general, $N_{\mathbf{n}}$ need not be the hopping neighbours $\{\mathbf{n}' : \tilde{t}_{\mathbf{n}\mathbf{n}'} \neq 0\}$. The low-energy sector for two electrons corresponds to dimer states (bipolarons) in which the electrons are on neighbouring sites; the energies in this sector are $V_{\min} + \mathrm{O}(\tilde{t})$. The energy cost of internal excitations of the bipolarons introduces a gap.

We can now sharply distinguish two types of bipolaron motion: 'crab-like', in which the constituent polarons remain neighbours, and 'crawler', which requires virtual transitions out of the low-energy sector. The crab-like bipolaron band width will be $O(\tilde{t})$, while the crawler contributions will be $O(\tilde{t}^2)$. We shall for the present purposes project onto the low-energy sector and hence ignore the resulting higher-order terms in $\tilde{t}$, immobilizing crawlers. For simplicity we absorb the polaron shift $-E_p$ into the chemical potential.

If a lattice Λ has L sites with a mean number ν of neighbours per site, then the single-polaron Hilbert space is $2L$-dimensional, the two-polaron Hilbert space is $4L^2$-dimensional and the crab bipolaron Hilbert space is just $4\nu L$-dimensional. We can further reduce to one singlet and three triplet spaces, each of dimensionality νL. The singlet bipolaron space is

$$\mathcal{S} = \text{span}\left\{\frac{1}{\sqrt{2}}\left(|\mathbf{n}\uparrow \mathbf{n}'\downarrow\rangle + |\mathbf{n}'\uparrow \mathbf{n}\downarrow\rangle\right) : \mathbf{n} \in \Lambda, \mathbf{n}' \in N_{\mathbf{n}}\right\} \tag{54}$$

and the $S_z = 1, 0, -1$ sectors of the triplet bipolaron space are

$$\mathcal{T}_1 = \text{span}\left\{|\mathbf{n}\uparrow \mathbf{n}'\uparrow\rangle : \mathbf{n} \in \Lambda, \mathbf{n}' \in N_{\mathbf{n}}\right\} \tag{55}$$

$$\mathcal{T}_0 = \text{span}\left\{\frac{1}{\sqrt{2}}\left(|\mathbf{n}\uparrow \mathbf{n}'\downarrow\rangle - |\mathbf{n}'\uparrow \mathbf{n}\downarrow\rangle\right) : \mathbf{n} \in \Lambda, \mathbf{n}' \in N_{\mathbf{n}}\right\} \tag{56}$$

$$\mathcal{T}_{-1} = \text{span}\left\{|\mathbf{n}\downarrow \mathbf{n}'\downarrow\rangle : \mathbf{n} \in \Lambda, \mathbf{n}' \in N_{\mathbf{n}}\right\}. \tag{57}$$

This enables us to write the low-energy effective Hamiltonian of the dimers in each sector as a tight-binding Hamiltonian on the *dimer lattice* constructed in the following way: a node is placed on the line joining neighbours in the lattice Λ. If $\mathbf{n}'$ and $\mathbf{n}''$ are both hopping neighbours of $\mathbf{n}$ ($\tilde{t}_{\mathbf{n}'\mathbf{n}''} \neq 0$), then the dimer can hop from $\mathbf{n}\mathbf{n}'$ to $\mathbf{n}\mathbf{n}''$. A bond is then drawn between the two nodes on the dimer lattice with hopping integral $\tilde{t}_{\mathbf{n}'\mathbf{n}''}$ in the singlet sector and $-\tilde{t}_{\mathbf{n}'\mathbf{n}''}$ in the triplet sector. This sign change ensures the correct exchange symmetry for closed paths on odd-membered rings: as a dimer completes one cycle of an odd-membered ring its end-points are interchanged. This can lead to a dramatic difference between singlet and triplet bipolaron masses on a non-bipartite lattice, as we shall see.

5.3. Ladders

In the staggered ladder depicted in figure 1 the neighbours of a site on one chain are the two adjacent sites on the opposite chain, while the hopping neighbours of a site are along the same chain. The corresponding dimer lattice is a one-dimensional chain with hopping $\pm\tilde{t}$ and two sites per unit cell. As there are no exchange paths, the sign of the hopping can be gauged away and there is no singlet–triplet splitting. The polaron and bipolaron dispersions are therefore respectively

$$E_p(k) = -\tilde{t}\cos ka, \tag{58}$$

$$E_{bp}(k) = \pm\tilde{t}\cos\frac{ka}{2}. \tag{59}$$

The bipolaron effective mass is therefore four times that of the polaron (as previously reported [9]):

$$m^* = \hbar^2 \left.\frac{\mathrm{d}^2 E_p(k)}{\mathrm{d}k^2}\right|_{k=0} = \frac{\hbar^2}{2\tilde{t}a^2}, \tag{60}$$

$$m^{**} = \hbar^2 \left.\frac{\mathrm{d}^2 E_{bp}(k)}{\mathrm{d}k^2}\right|_{k=0} = \frac{2\hbar^2}{\tilde{t}a^2}. \tag{61}$$

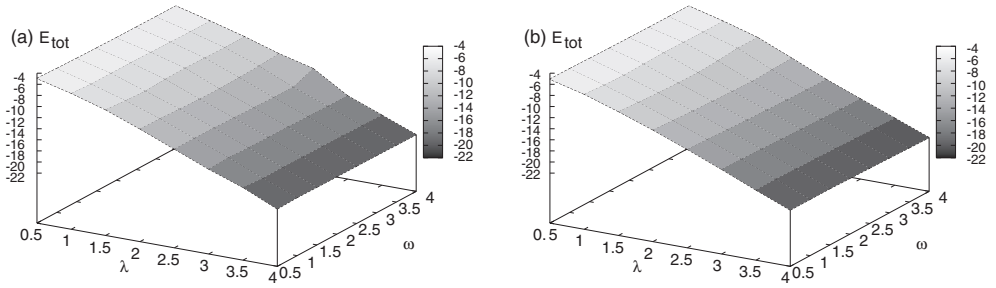

Figure 5. Total energy of the bipolaron for (a) the rectangular ladder and (b) the staggered ladder. A slight change in gradient between weak and strong coupling is just discernable, demonstrating (as we shall see in the coming figures) that the staggered ladder reaches the strong-coupling limit at significantly lower λ than the rectangular ladder. Here $R_{sc} = 1$.

This result is remarkable if one considers the standard strong coupling result for the mass of the bipolaron. In the rectangular ladder the requirement for a virtual internal excitation of the bipolaron in the crawler dynamics would lead to a hopping $O(\tilde{t}^2)$ and hence mass $O((m^*)^2)$. The staggered ladder with long-range electron phonon attraction has two degenerate nearest-neighbour bound states (as summarized in figure 12), so no intermediate state is required when the particle hops. It is clearly important that the electrons are bound one lattice spacing apart to take advantage of this effect, but this can easily be achieved in the presence of a strong site-local Coulomb repulsion (so that the energy is not at a minimum when both particles are on the same site). This spaced minimum is clearly extremely important when real lattices beyond the toy ladder models presented here are considered. Some details of real lattices will be discussed later in this paper, but to briefly summarize, in order to obtain this special kind of bipolaron: (a) the lattice must have several degenerate near-neighbour bound states which can be transformed from one degenerate state to another via a single hop; (b) strong Coulomb repulsion is required to stop a unique single-site bound state from forming between the polarons, and (c) long-range attraction is required so that the minimum in the potential function (attraction + repulsion) is at approximately one lattice spacing. This information is summarized in figures 12 and 13 in the conclusion to this paper.

5.4. QMC

We compute QMC results for bipolarons moving on staggered and rectangular ladders with period 1000 for a range of λ and ω, including the total energy, inverse bipolaron mass, bipolaron radius, mass isotope exponent and the number of phonons in the bipolaron cloud. Figure 5 shows the total energy of the bipolaron for (a) the rectangular ladder and (b) the staggered ladder. A slight change in gradient between weak and strong coupling is just discernable, demonstrating (as we shall see in the coming figures) that the staggered ladder reaches the strong-coupling limit at significantly lower λ than the rectangular ladder. Strong-coupling results from the previous section agree well. We see that there are no significant differences between the total energy of the bipolarons on the staggered and rectangular ladders, although the strong-coupling limit is reached for slightly lower λ in the case of the staggered ladder.

If one is to reach a superconducting state via the Bose–Einstein condensation of bipolarons, there are two conditions. First, the bipolaron pair must be light, and second, the pairing radius must be small. We demonstrate the differences between the inverse masses on the staggered and rectangular ladders in figures 6(a) and (b), which show the inverse mass of the bipolaron

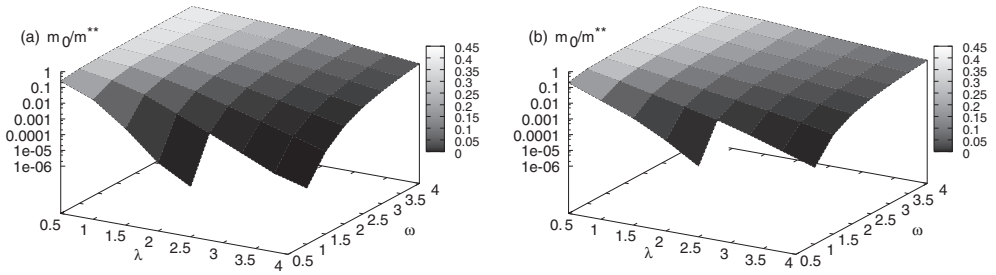

Figure 6. Inverse mass of the bipolaron for (a) the rectangular ladder and (b) the staggered ladder. There is more than an order of magnitude difference between the mass of the bipolaron on the staggered ladder, and that on the rectangular ladder over significant regions of the parameter space. Bipolaron masses on the staggered ladder have recently been shown to have a value commensurate with the polaron mass. Here $R_{sc} = 1$.

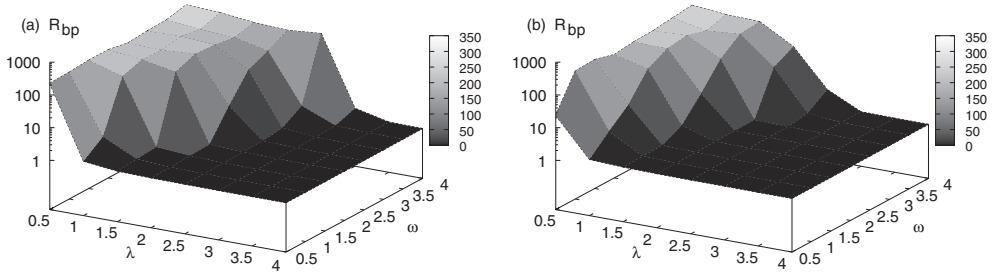

Figure 7. Size of the bipolaron for (a) the rectangular ladder and (b) the staggered ladder. Not only is the bipolaron on the staggered ladder lighter than that on the rectangular ladder, but its size is also smaller for equivalent λ. Here $R_{sc} = 1$.

for a number of different λ and ω/t. There is more than an order of magnitude difference between the mass of the bipolaron on the staggered ladder, and that on the rectangular ladder over significant regions of the parameter space. In fact, the magnitude of the bipolaron mass turns out to be of similar size to that of the polaron mass over a wide range of the parameter space. The mass is inversely proportional to the transition temperature of the BEC, so a small mass is essential to obtain a decent T_C.

We have demonstrated that one of the precursors for a Bose–Einstein condensate of pairs above the mK range may be met on the staggered ladder arrangement, but we also require small pairs, with non-overlapping wavefunctions. In figure 7 we show how the size of the bipolaron varies as λ and ω/t are varied. Not only is the bipolaron on the staggered ladder lighter than that on the rectangular ladder, but it also has a significantly smaller radius than the bipolaron on the rectangular ladder, making it a much better prospect for Bose–Einstein condensation.

Since the result that the bipolaron mass is proportional to the polaron mass via a numerical value relies on the anti-adiabatic limit, where the phonon frequency is very large, so that phonons may not be excited, we investigate the number of phonons associated with the bipolaron in figure 8. The result is weighted by phonon frequency and electron–phonon coupling, so that the strong-coupling result can clearly be seen. Again, we can see that the strong-coupling limit is reached at significantly lower λ on the staggered ladder than on the rectangular ladder. Strong-coupling results from the previous section agree well, with the ratio $\bar{\omega}N_{ph}/\lambda$ approaching the numerical value given in table 1. The anti-adiabatic limit can clearly be identified as regions on the graph where the phonon number approaches

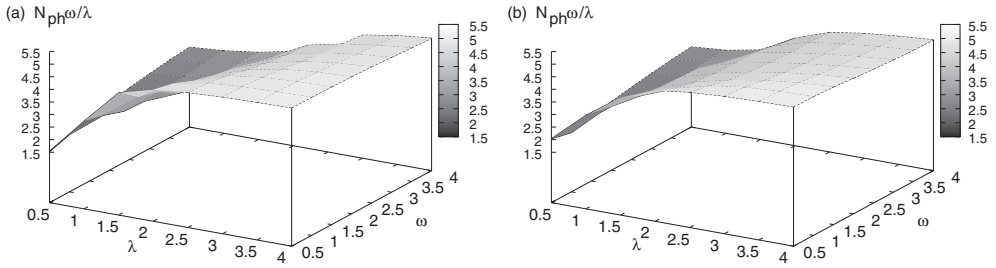

Figure 8. Number of phonons associated with the bipolaron for (a) the rectangular ladder and (b) the staggered ladder, weighted by phonon frequency and electron–phonon coupling. Again, we can see that the strong-coupling limit is achieved at significantly lower λ on the staggered ladder. It is interesting to note that the states with large omega have a smaller number of phonons. This is consistent with the anti-adiabatic approximation: when the phonon frequency is large, creating phonons becomes difficult, and the phonon wavefunction is the vacuum state. Then the phonon problem maps onto a UV model (discussed later). Here $R_{sc} = 1$.

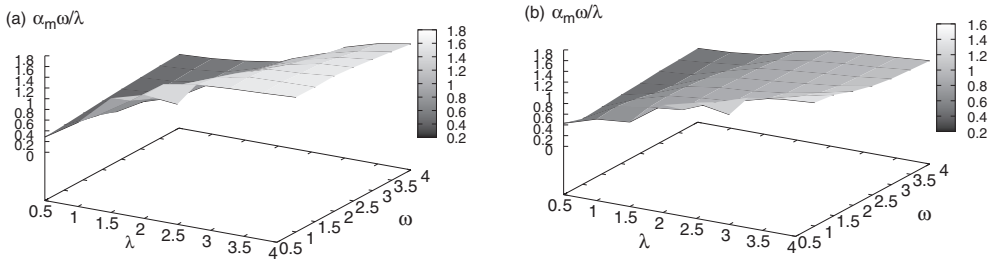

Figure 9. Mass isotope exponent of the bipolaron for (a) the rectangular ladder and (b) the staggered ladder. Again, we can see that the strong-coupling limit is achieved at significantly lower λ on the staggered ladder. The isotope exponent is also smaller on the staggered ladder, demonstrating a much smaller range of mass from weak to strong coupling. Here $R_{sc} = 1$.

zero (i.e. the $\omega > \lambda$ quadrant of the parameter space), consistent with results for the mass.

We show the mass isotope exponent of the bipolaron in figure 9. Again, we can see that the strong-coupling limit is achieved at significantly lower λ on the staggered ladder, compared with the rectangular ladder. The isotope exponent is also smaller on the staggered ladder, demonstrating a much smaller range of mass from weak to strong coupling.

Finally, in figure 10, we show example path configurations on (a) the rectangular ladder and (b) the staggered ladder. Hopping events on different paths on the rectangular ladder are very closely correlated on the imaginary time axis. On the staggered ladder, there are two degenerate configurations, and paths are just as likely to sit on either of the two neighbouring sites, significantly reducing the correlation between kinks, and increasing the probability that kink pairs can be inserted. It is this that leads to significantly lighter bipolarons on the staggered ladder.

6. Beyond ladders: other superlight systems

On the ladder systems, the electrons were held on neighbouring legs of the ladders. This is partially consistent with a very strong local Coulomb repulsion or Hubbard U. It is also possible to examine the effects of a very strong or even infinite Hubbard U on the masses of

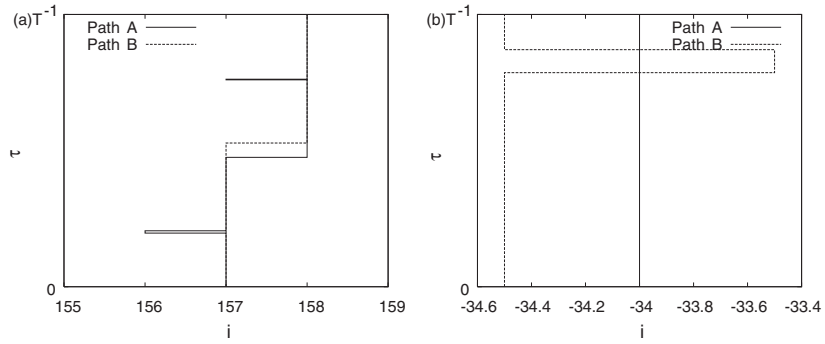

Figure 10. Example path configurations on (a) the rectangular ladder and (b) the staggered ladder. Hopping events on different paths on the rectangular ladder are very correlated in time. On the staggered ladder, there are two degenerate configurations, and paths are just as likely to sit on either of the two neighbouring sites, significantly reducing the correlation between kinks. ($\omega/t = \lambda = 4$ in both cases.)

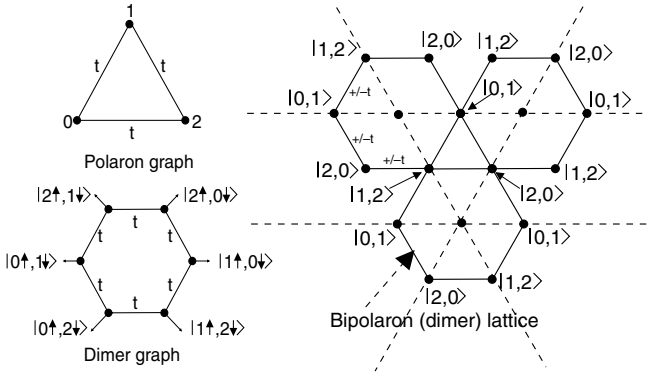

Figure 11. The triangular lattice (thin lines) with a dimer state (circle) at the mid-point of each bond. The polaron and bipolaron states are indicated on one triangle, with spin indices suppressed. The dimer lattice (thick lines) is a kagome lattice.

bipolarons bound via long-range attraction on other low-dimensional systems. As we have seen by examining the ladder systems, there are three requirements for superlight bipolarons: (1) electrons are not allowed to bind on a single site; (2) there are at least two degenerate configurations of electrons sitting on neighbouring sites, and (3) there are single hopping events which transform one configuration into another degenerate configuration. Then, hopping of the bipolaron is first order in the hopping of the polaron. Condition (2) is satisfied by long-range electron–phonon interaction, and there are several tight-binding lattices which also satisfy conditions (2) and (3), and a strong site-local Coulomb repulsion satisfies condition (1). We discuss bipolarons on these lattices in the anti-adiabatic approximation in this section.

6.1. Triangular molecule

The staggered ladder system discussed earlier in this paper can be considered to be made up of triangular plaquettes, so the first logical step to looking beyond the ladder systems is to analyse the physics of a single plaquette. If hopping is allowed between all the sites on the plaquette, then one may consider exchange effects, which lead to singlet and triplet bound states. To

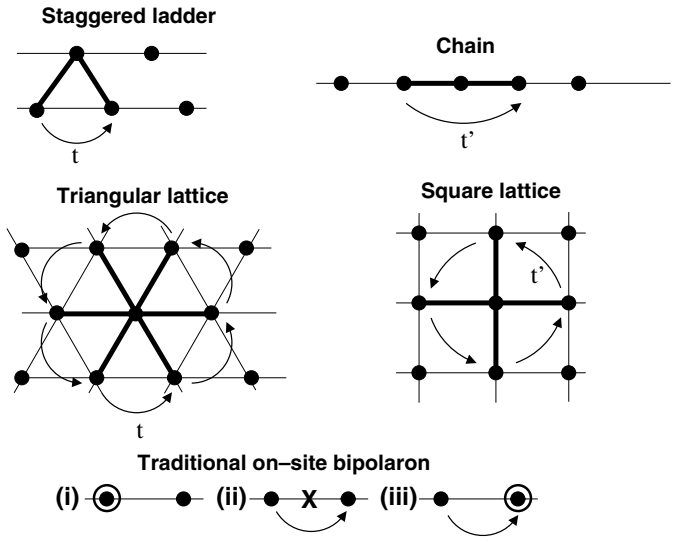

Figure 12. Pictorial demonstration of lattices which are expected to lead to superlight and light bipolarons when long-range electron–phonon interaction is present in combination with a strong site-local Coulomb repulsion (Hubbard U) which stops on-site binding. All degenerate nearest-neighbour bound states are shown as the thick lines. The lightest bipolarons are expected on lattices with a triangular component, where hopping between degenerate states can be realized with the same single hop as the polaron (shown as arrows). Thus the bipolaron moves in the first order of the polaron mass. We also show potential single hops for light bipolarons on the chain, and the square lattice, which can be realized if next-nearest-neighbour hopping is present. The superlight bipolarons are contrasted with traditional (Holstein) on-site bipolarons, which move with two hopping events, the first one breaking the bound state (step (ii)), and the second reforming it (step (iii)); thus such on-site (crawler) bipolarons cannot be simultaneously small (well-bound) and mobile.

see exchange effects, we require lattices with odd-membered rings. As the simplest example, consider three sites $0, 1, 2$, all of which are neighbours, with hopping $\tilde{t} > 0$. The polaron Hamiltonian is

$$H = \begin{pmatrix} 0 & -\tilde{t} & -\tilde{t} \\ -\tilde{t} & 0 & -\tilde{t} \\ -\tilde{t} & -\tilde{t} & 0 \end{pmatrix}. \tag{62}$$

The dimer lattice is constructed by placing a node at the centre of each bond. The singlet bipolaron Hamiltonian is therefore

$$H_{\mathrm{S}} = \begin{pmatrix} V_{\mathrm{min}} & -\tilde{t} & -\tilde{t} \\ -\tilde{t} & V_{\mathrm{min}} & -\tilde{t} \\ -\tilde{t} & -\tilde{t} & V_{\mathrm{min}} \end{pmatrix} \tag{63}$$

with eigenvalues $\{V_{\mathrm{min}} - 2\tilde{t}, V_{\mathrm{min}} + \tilde{t}, V_{\mathrm{min}} + \tilde{t}\}$, and the triplet bipolaron Hamiltonian is

$$H_{\mathrm{T}} = \begin{pmatrix} V_{\mathrm{min}} & \tilde{t} & \tilde{t} \\ \tilde{t} & V_{\mathrm{min}} & \tilde{t} \\ \tilde{t} & \tilde{t} & V_{\mathrm{min}} \end{pmatrix} \tag{64}$$

with eigenvalues $\{V_{\mathrm{min}} - \tilde{t}, V_{\mathrm{min}} - \tilde{t}, V_{\mathrm{min}} + 2\tilde{t}\}$. (An alternative choice of basis would be the six-dimensional unsymmetrized $S_z = 0$ basis $\{|i\uparrow j\downarrow\rangle\}$. This would transform the triangle into a

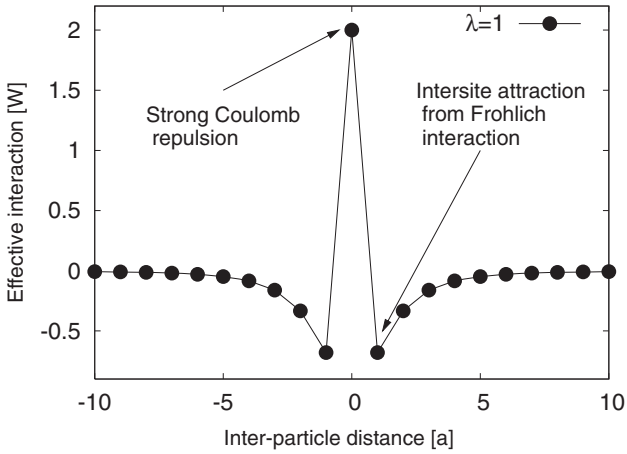

Figure 13. Pictorial demonstration of the inter-polaron effective interaction which can lead to superlight bipolarons (cross-section of anti-adiabatic limit of triangular lattice with $\lambda = 1$). A strong on-site Coulomb repulsion (Hubbard U) stops on-site binding, leading to binding between polarons on neighbouring sites when there is a long-range phonon-mediated attraction. In this case, the potential well should lead to binding of small bipolarons on the order of one lattice parameter. The long-range Fröhlich electron–phonon attraction may be found on quasi-two-dimensional lattices, where ions oscillate above planes (as described in [9]).

six-member ring. Such a basis becomes unwieldy for typical lattices.) Clearly, the properties of the plaquette are defined by single-polaron hopping events, since there are no eigenvalues with $\mathrm{O}(\tilde{t}^2)$ terms. It is this property which makes lattices which can be constructed from triangular plaquettes a good starting place when looking for small superlight bipolarons.

6.2. Triangular lattice

Let us consider a triangular lattice with nearest-neighbour hopping t. In the anti-adiabatic approximation, this is replaced by $\tilde{t}$. The polaron band structure (ignoring polaron shift) is $E(\mathbf{k}) = -2\tilde{t}C(\mathbf{k})$, where we have defined

$$C(\mathbf{k}) \equiv \cos k_x a + \cos\left(k_x a/2 - \sqrt{3}k_y a/2\right) + \cos\left(k_x a/2 + \sqrt{3}k_y a/2\right), \tag{65}$$

a being the lattice parameter. Expanding near the Γ point gives

$$E(\mathbf{k}) = -6\tilde{t} + \tfrac{3}{2}k^2 a^2 \tilde{t} + \mathrm{O}(k^4). \tag{66}$$

The polaron effective mass is therefore

$$m^* = \frac{\hbar^2}{3\tilde{t}a^2}. \tag{67}$$

By placing a node on each bond in the lattice, we see that the resulting dimer lattice is a kagome lattice. The dispersion is easily found as follows, (see also [25]) by diagonalizing the secular matrix

$$H(\mathbf{k}) = V_{\min} \mp \tilde{t} \begin{vmatrix} 0 & 1+\gamma^* & 1+\beta \\ 1+\gamma & 0 & 1+\alpha^* \\ 1+\beta^* & 1+\alpha & 0 \end{vmatrix}, \tag{68}$$

with

$$\alpha = \exp\left(-\mathrm{i}k_x a/2 + \mathrm{i}\sqrt{3}k_y a/2\right) \tag{69}$$

$$\beta = \exp\left(-\mathrm{i}k_x a/2 - \mathrm{i}\sqrt{3}k_y a/2\right) \tag{70}$$

$$\gamma = \exp\left(\mathrm{i}k_x a\right). \tag{71}$$

The sign in (68) is $-\tilde{t}$ for the singlet and $+\tilde{t}$ for the triplet. There are three bipolaron bands with no gaps:

$$E_1(\mathbf{k}) = V_{\min} \pm \tilde{t}\left(-1 - \sqrt{3 + 2C(\mathbf{k})}\right) \tag{72}$$

$$E_2(\mathbf{k}) = V_{\min} \pm \tilde{t}\left(-1 + \sqrt{3 + 2C(\mathbf{k})}\right) \tag{73}$$

$$E_3(\mathbf{k}) = V_{\min} \pm 2\tilde{t}. \tag{74}$$

with sign $+\tilde{t}$ for the singlet and $-\tilde{t}$ for the triplet.

The lowest singlet band is

$$E_1(\mathbf{k}) = V_{\min} - 4\tilde{t} + \tfrac{1}{4}k^2a^2\tilde{t} + \mathrm{O}(k^4), \tag{75}$$

with effective mass

$$m_{\mathrm{s}}^{**} = \frac{2\hbar^2}{\tilde{t}a^2} = 6m^*. \tag{76}$$

We notice that this increases *linearly* with the polaron mass, indicating that crab-like bipolarons can be relatively light.

The lowest triplet band is the *flat band* $E_3(\mathbf{k}) = V - 2\tilde{t}$. This implies that a triplet crab-like bipolaron has *infinite* mass on a triangular lattice. Once crawler motion is permitted, the effective mass is expected to be finite but proportional to $(m^*)^2$.

6.3. Lattices with long-range hopping

Lattices with triangular components are not the only ones where the ability to move between degenerate paired states can be utilized to lead to small masses. For example, if we introduce next-nearest-neighbour hopping to a linear chain, then, in the anti-adiabatic approximation, we obtain a bipolaron inverse mass, $2(2a)^2\tilde{t}'$, and a polaron inverse mass, $2a^2\tilde{t}$, where $\tilde{t} = t\exp(-W\lambda(1 - \Phi(0,\mathbf{a})/\Phi(0,0))/\omega)$ and $\tilde{t}' = t'\exp(-W\lambda(1 - \Phi(0,2\mathbf{a})/\Phi(0,0))/\omega)$. While this does not lead to an exact cancellation of the exponents, the bipolaron to polaron inverse mass ratio is linear in t'/t, and the bipolaron is therefore expected to be light.

Another suggestion for bipolarons with light mass comes from the cuprate lattice. It has often been suggested that the tight-binding structure of the cuprates is a square lattice with nearest-neighbour hopping t and next-nearest-neighbour hopping t'. In the presence of very strong Coulomb repulsion U, one may determine that the ground state of the Lang–Firsov transformed Hamiltonian consists of nearest-neighbour pairs with degeneracy four. If one applies the anti-adiabatic approximation to such a lattice, one determines that the hopping of such a bipolaron is first order in t'. We obtain a bipolaron inverse mass, $2(\sqrt{2}a)^2\tilde{t}'$, and a polaron inverse mass, $2a^2\tilde{t}$, where $\tilde{t} = t\exp(-W\lambda(1 - \Phi(0,\mathbf{a})/\Phi(0,0))/\omega)$ and $\tilde{t}' = t'\exp(-W\lambda(1 - \Phi(0,\mathbf{a} - R^{90}\mathbf{a})/\Phi(0,0))/\omega)$. Here R^{90} is the rotation operator. Again, while we do not get an exact cancellation of the exponents, we obtain a resulting inverse mass ratio proportional to t'/t, and light bipolarons are likely[4]. Such pairing is an appealing prospect, especially since Hague has demonstrated the potential for d-wave superconductivity mediated by Holstein-like electron–phonon interactions in the intermediate coupling limit [29].

[4] It is interesting to note that these lattices share a common feature with triangular lattices, namely that it is possible for a single particle to hop three times to return to the point of origin, indicating a more universal prospect for this phenomenon.

7. Conclusions

The bipolaronic extension [4] of the BCS theory towards the strong interaction between electrons and ion vibrations proved that the Cooper pairing in momentum space [1] and the Ogg–Schafroth real-space pairing [27, 28] are two extreme limits of the same problem. For a very strong electron–phonon coupling, polarons become self-trapped on a single lattice site and bipolarons are on-site singlets. In the Holstein model of the zero-range EPI their mass appears only in the second order of polaron hopping [18], so that on-site bipolarons are very heavy. This estimate led some authors to the conclusion that the formation of itinerant small polarons and bipolarons in real materials is unlikely [30], and high-temperature bipolaronic superconductivity is impossible [31].

In fact, we have demonstrated here that small but light bipolarons could exist for realistic values of the finite-range EPI with high-frequency optical phonons in staggered ladder systems. Small light bipolarons are an essential precursor to high-temperature superconductivity, since the Bose–Einstein condensate has a transition temperature that is inversely proportional to mass, and wavefunctions may not overlap. Such bipolarons are easily formed on lattices with triangular plaquettes in the presence of extremely large on-site Coulomb repulsion, and persist to large EPI. This conclusion is backed up by analytics in the anti-adiabatic approximation in the presence of large intersite Coulomb attraction. Another important conclusion is that the triplet–singlet exchange energy is of the first order in the hopping integral, and triplet bipolarons are heavier than singlets in certain lattice structures at variance with simple intuitive expectations. We summarize the types of lattices where light 'crab' bipolarons may be formed in figure 12, contrasting with the traditional Holstein bipolarons (bottom), and describe the required effective interaction in figure 13, demonstrating the underlying physics of such bipolarons.

Our CTQMC simulations lead us to believe that the following recipe is worth investigating to look for very high-temperature superconductivity: (a) the parent compound should be an ionic insulator with light ions to form high-frequency optical phonons, (b) the structure should be quasi-two-dimensional to ensure poor screening of high-frequency c-axis polarized phonons, (c) a triangular lattice is required in combination with strong, on-site Coulomb repulsion to form the small superlight Crab bipolaron, and (d) moderate carrier densities are required to keep the system of small bipolarons close to the dilute regime. Many of these conditions are already met in the cuprates.

Acknowledgments

We would like to acknowledge EPSRC (grant numbers EP/C518365/1 and EP/D07777X/1). While writing this article, conversations with Serge Aubry, Peter Edwards, Janez Bonča, Jozef Devreese, Holger Fehske, Yurii Firsov, Martin Hohenadler, Viktor Kabanov, Wolfgang von der Linden, Peter Littlewood, Dragan Mihailovic, Arndt Simon, Marshall Stoneham, and other participants of the European Science Foundation workshop 'Mott's Physics in Nanowires and Quantum Dots' (Cambridge, UK, 31 July–2 August, 2006) were especially helpful. We acknowledge support from Loughborough University, Gonville and Caius College, Cambridge University and the ESF for this workshop.

References

[1] Bardeen J, Cooper L N and Schrieffer J R 1957 *Phys. Rev.* **108** 1175
[2] Alexandrov A S and Mott N F 1994 *Rep. Prog. Phys.* **57** 1197

[3] Alexandrov A S and Edwards P P 2000 *Physica* C **331** 97
[4] Alexandrov A S 2003 *Theory of Superconductivity: From Weak to Strong Coupling* (Bristol: Institute of Physics Publishing)
[5] Edwards P P, Rao C N R, Kumar N and Alexandrov A S 2006 *ChemPhysChem* **7** 2015
[6] Alexandrov A S 1996 *Phys. Rev.* B **53** 2863
[7] Anderson P W, Lee P A, Randeria M, Rice T M, Trivedi N and Zhang F C 2004 *J. Phys.: Condens. Matter* **16** R755
[8] Kim J H, Feenstra B J, Somal H S, van der Marel D, Lee W Y, Gerrits A M and Wittlin A 1994 *Phys. Rev.* B **49** 13065
[9] Alexandrov A S and Kornilovitch P E 2002 *J. Phys.: Condens. Matter* **14** 5337
[10] Zhao G and Morris D E 1995 *Phys. Rev.* B **51** 16487
Zhao G-M, Hunt M B, Keller H and Müller K A 1997 *Nature* **385** 236
Khasanov R, Eshchenko D G, Luetkens H, Morenzoni E, Prokscha T, Suter A, Garifianov N, Mali M, Roos J, Conder K and Keller H 2004 *Phys. Rev. Lett.* **92** 057602
[11] Alexandrov A S 1992 *Phys. Rev.* B **46** 14932
[12] Lanzara A, Bogdanov P V, Zhou X J, Kellar S A, Feng D L, Lu E D, Yoshida T, Eisaki H, Fujimori A, Kishio K, Shimoyana J I, Noda T, Uchida S, Hussain Z and Shen Z X 2001 *Nature* **412** 510
Gweon G H, Sasagawa T, Zhou S Y, Craf J, Takagi H, Lee D H and Lanzara A 2004 *Nature* **430** 187
[13] Meevasana W, Ingle N J C, Lu D H, Shi J R, Baumberger F, Shen K M, Lee W S, Cuk T, Eisaki H, Devereaux T P, Nagaosa N, Zaanen J and Shen Z-X 2006 *Phys. Rev. Lett.* **96** 157003
[14] Lee J, Fujita K, McElroy K, Slezak J A, Wang M, Aiura Y, Bando H, Ishikado M, Masui T, Zhu J X, Balatsky A V, Eisaki H, Uchida S and Davis J C 2006 *Nature* **442** 546
[15] Mihailovic D, Foster C M, Voss K and Heeger A J 1990 *Phys. Rev.* B **42** 7989
Calvani P, Capizzi M, Lupi S, Maselli P, Paolone A, Roy P, Cheong S W, Sadowski W and Walker E 1994 *Solid State Commun.* **91** 113
Zamboni R, Ruani G, Pal A J and Taliani C 1989 *Solid State Commun.* **70** 813
[16] Sendyka T R, Dmowski W and Egami T 1995 *Phys. Rev.* B **51** 6747
Egami T 1996 *J. Low Temp. Phys.* **105** 791
[17] Verbist G, Peeters F M and Devreese J T 1991 *Phys. Rev.* B **43** 2712
Verbist G, Peeters F M and Devreese J T 1990 *Solid State Commun.* **76** 1005
[18] Alexandrov A S and Ranninger J 1981 *Phys. Rev.* B **23** 1796
Alexandrov A S and Ranninger J 1981 *Phys. Rev.* B **24** 1164
Under certain conditions relatively mobile intersite bipolarons can be found even in the Holstein–Hubbard model, generally unfavourable for coherent tunnelling, see La Magna A and Pucci R 1997 *Phys. Rev.* B **55** 14886
Proville L and Aubry S 1999 *Eur. Phys. J.* B **11** 41
Bonča J, Katrasnic T and Trugman S A 2000 *Phys. Rev. Lett.* **84** 3153
Macridin A, Sawatzky G A and Jarrell M 2004 *Phys. Rev.* B **69** 245111
[19] Kornilovitch P E 1998 *Phys. Rev. Lett.* **81** 5382
Kornilovitch P E 1999 *Phys. Rev.* B **60** 3237
[20] Spencer P E, Samson J H, Kornilovitch P E and Alexandrov A S 2005 *Phys. Rev.* B **71** 184310
[21] Hague J P, Kornilovitch P E, Alexandrov A S and Samson J H 2006 *Phys. Rev.* B **73** 054303
[22] Hague J P, Kornilovitch P E, Samson J H and Alexandrov A S 2007 *Phys. Rev. Lett.* **98** 037002
Hague J P, Kornilovitch P E, Alexandrov A S and Samson J H 2007 *Physica* C (*Preprint* cond-mat/0606719)
[23] Lang I G and Firsov Yu A 1962 *Zh. Eksp. Teor. Fiz.* **43** 1843
Lang I G and Firsov Yu A 1963 *Sov. Phys.—JETP* **16** 1301 (Engl. Transl.)
[24] Tyablikov S V 1951 *Zh. Eksp. Teor. Fiz.* **21** 377
Tyablikov S V 1952 *Zh. Eksp. Teor. Fiz.* **23** 381 (in Russian)
[25] Xiao Y, Pelletier V, Chaikin P M and Huse D A 2003 *Phys. Rev.* B **67** 104505
[26] Kornilovitch P E 2007 *J. Phys.: Condens. Matter* **19** 255206
[27] Ogg R A Jr 1946 *Phys. Rev.* **69** 243
[28] Schafroth M R 1955 *Phys. Rev.* **100** 463
Blatt J M and Butler S T 1955 *Phys. Rev.* **100** 476
[29] Hague J P 2006 *Phys. Rev.* B **73** 060503(R)
Hague J P 2005 *J. Phys.: Condens. Matter* **17** 5663
Hague J P 2003 *J. Phys.: Condens. Matter* **15** 2535
[30] de Mello E V L and Ranninger J 1998 *Phys. Rev.* B **58** 9098
[31] Anderson P W 1997 *The Theory of Superconductivity in the Cuprates* (Princeton, NJ: Princeton University Press)